MATERIALS SCIENCE

Free-standing liquid membranes as unusual particle separators

Birgitt Boschitsch Stogin[1,2], Luke Gockowski[1], Hannah Feldstein[1], Houston Claure[1], Jing Wang[1,2], Tak-Sing Wong[1,2,3]*

Copyright © 2018 The Authors, some rights reserved; exclusive licensee American Association for the Advancement of Science. No claim to original U.S. Government Works. Distributed under a Creative Commons Attribution NonCommercial License 4.0 (CC BY-NC).

Separation of substances is central to many industrial and medical processes ranging from wastewater treatment and purification to medical diagnostics. Conventional solid-based membranes allow particles below a critical size to pass through a membrane pore while inhibiting the passage of particles larger than that critical size; membranes that are capable of showing reversed behavior, that is, the passage of large particles and inhibition of small ones, are unusual in conventional engineering applications. Inspired by endocytosis and the self-healing properties of liquids, we show that free-standing membranes composed entirely of liquid can be designed to retain particles smaller than a critical size given the particle inertial properties. We further demonstrate that these membranes can be used for previously unachievable applications, including serving as particle barriers that allow macroscopic device access through the membrane (for example, open surgery) or as selective membranes inhibiting gas/vapor passage while allowing solids to pass through them (for example, waste/odor management).

INTRODUCTION

For centuries, particle separation has been a process of great significance. Today, its importance spans across several fields ranging from medical diagnostics (*1*) to wastewater treatment and water desalination (*2*). Some of the simplest separation techniques are sieving and filtration —processes that rely on membranes that allow certain particles to pass through them while preventing the passage of others. Conventional membranes are porous and allow particles smaller than a typical pore size to pass through the pores while retaining those larger than the pore size. Membranes that allow relatively large particles to pass while retaining smaller ones, however, are counterintuitive and uncommon. While unusual in human practice, membranes with these capabilities are readily found in nature. Cells, for example, are encased by a phospholipid bilayer composed of amphiphilic molecules that can dynamically reconfigure themselves (*3*, *4*). This property, in conjunction with other biological mechanisms, makes possible the engulfment of large particles without fluid exchange as exemplified by endocytosis.

As displayed in nature, membranes that allow large particles to pass while retaining small ones must be dynamically reconfigurable and self-healing—properties commonly exhibited by liquids. While liquids have many unique materials properties, membrane engineering efforts have predominantly focused on solid-based materials. In recent years, the concept of incorporating liquids into solid-based materials has led to breakthrough surface technologies (*5*–*9*). For example, the incorporation of stable liquid layers into porous solids allows self-healing, robust liquid repellency (*5*), anti-biofouling (*6*), anti-icing (*7*), and even gating (*9*) properties. Despite the unique materials properties of liquids (for example, rapid self-healing), the concept of using membranes composed entirely of liquids as functional materials has remained unexplored (Fig. 1A).

Here, we show that free-standing membranes composed purely of liquids can achieve particle separation regimes that cannot be attained by conventional membrane technologies (Fig. 1, B and C). Specifically, by tuning the membrane surface tension and geometric parameters, we demonstrate that one can design a membrane that can retain particles smaller than a critical size based on the particle inertial properties. Further, we have demonstrated that the unique properties of liquid membranes allow applications that were previously unachievable by conventional membrane technologies, including entrapment of microscopic entities while allowing the passage of macroscopic objects, and selective gas-solid separation where the membrane allows solids to pass through while inhibiting gas passage.

[1]Department of Mechanical and Nuclear Engineering, Pennsylvania State University, University Park, PA 16802, USA. [2]Materials Research Institute, Pennsylvania State University, University Park, PA 16802, USA. [3]Department of Biomedical Engineering, Pennsylvania State University, University Park, PA 16802, USA.
*Corresponding author. Email: tswong@psu.edu

RESULTS

Design principles

Liquid membranes consist of a stabilized liquid material that can be as simple as a two-component system [for example, water and surfactant—a soap film (*10*–*12*)] or a complex multicomponent system designed for a specific application. The simplest stabilized liquid membrane can be prepared by mixing deionized water with varying concentrations of surfactant [for example, sodium dodecyl sulfate (SDS)]. Subsequently, a solid ring can be used to support a free-standing liquid membrane. By varying the concentration of SDS, we can tune the film surface tension from ~35 to ~72 mN/m. When two spheres with identical materials properties but of different sizes are released from a fixed height H onto a liquid membrane with a surface tension γ, one will notice that, at certain values of H, the larger sphere will pass through the membrane and the smaller sphere will be retained within the membrane (Fig. 2A and movie S1) (*11*, *12*). On the basis of this experimental observation, we can categorize the particle-membrane interactions in two different regimes: (i) the particle retention regime and (ii) the particle "pass-through" regime.

To experimentally determine the mechanisms that dictate whether a particle will pass through or remain in the film, we systematically dropped beads into a liquid membrane of a given surface tension from different heights and recorded whether the bead was retained in or passed through the membrane. Specifically, we dropped relatively smooth beads (root mean square roughness, $\xi < 2.5\ \mu m$) into a stabilized liquid membrane of a given surface tension and radius from heights H ranging from 0.5 to 15 cm (tables S1 to S3). Typical particle impact velocities u_b were <2 m/s. We repeated this experiment using liquid membranes with different surface tensions ($35\ mN/m < \gamma < 72\ mN/m$). To test for the effect of particle geometry on retention/pass-through, we

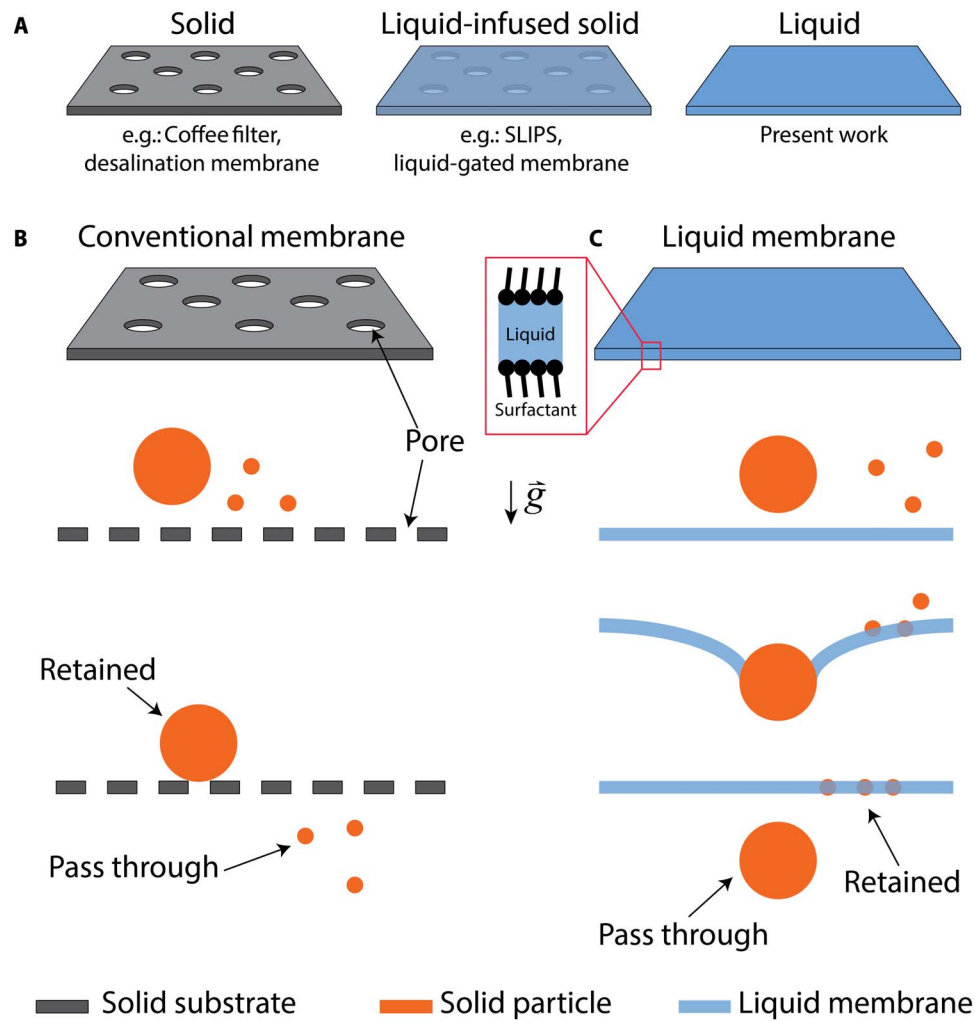

Fig. 1. Concept of liquid membrane. (**A**) Schematics showing the materials architectural differences between solid membranes, liquid-infused porous materials [for example, slippery liquid-infused porous surfaces (SLIPS) (*5*)], and the liquid membrane presented in the current work. (**B**) Conventional solid membranes use porous geometries to allow small particles to pass through while mechanically inhibiting the passage of large particles. (**C**) Liquid membranes rely on entirely different mechanisms for particle separation and allow reversed separation behavior: Small particles can be retained, while large ones pass through the membrane.

conducted the same set of experiments for beads and membranes of different radii (355 μm< R_b <4.4 mm and 3 mm< R_f <6 cm, respectively). Further testing was carried out using beads composed of different materials [that is, glass, polystyrene (PS), and polytetrafluoroethylene (PTFE)] to investigate the effect of surface chemistry on the particle-membrane interaction.

To gain physical insights into the particle separation mechanism, we compared the magnitudes of the kinetic energy (E_{u_b}) of the beads at impact to the other forms of energy, such as the maximum increase in film surface energy due to stretching (E_S) (*12*) and energy dissipation (E_{diss}) due to film pinning (E_P) at the bead boundary (section S2 and figs. S1 and S2)

$$E^* = \frac{E_S + E_{diss}}{E_{u_b}} \quad (1)$$

Note that, in our particular experiments, the capillary number *Ca* was small (that is, $Ca \sim 10^{-2}$), indicating that the viscous effects were less significant than the surface tension effects and were therefore neglected. In addition, it has been shown that the films will form a catenoid shape (*13*) when slow-moving particles impact liquid films (that is, Weber number, $We < 3200$; our particles impacted the membranes at <2 m/s). Therefore, the maximum change in surface energy (E_S) due to the film stretching was approximated to be the difference between the maximum area the film can stretch and the area of the flat film of outer radius R_f (that is, the radius of the liquid membrane) and inner radius R_b (that is, the radius of the spherical impacting particle; section S2). This change in surface energy can be approximated as

$$E_S = \pi\gamma\left\{R_b^2[\sinh\phi + \phi] - 2(R_f^2 - R_b^2)\right\} \quad (2)$$

where $\phi = 2\cosh^{-1}\left(\frac{R_f}{R_b}\right)$. Furthermore, we estimated the energy loss due to pinning (E_P) based on our experimental parameters and found this term to be negligible in our experiments. Therefore, E^* can be reduced to the following equation for our experiments

$$E^* \approx \gamma C / E_{u_b} \quad (3)$$

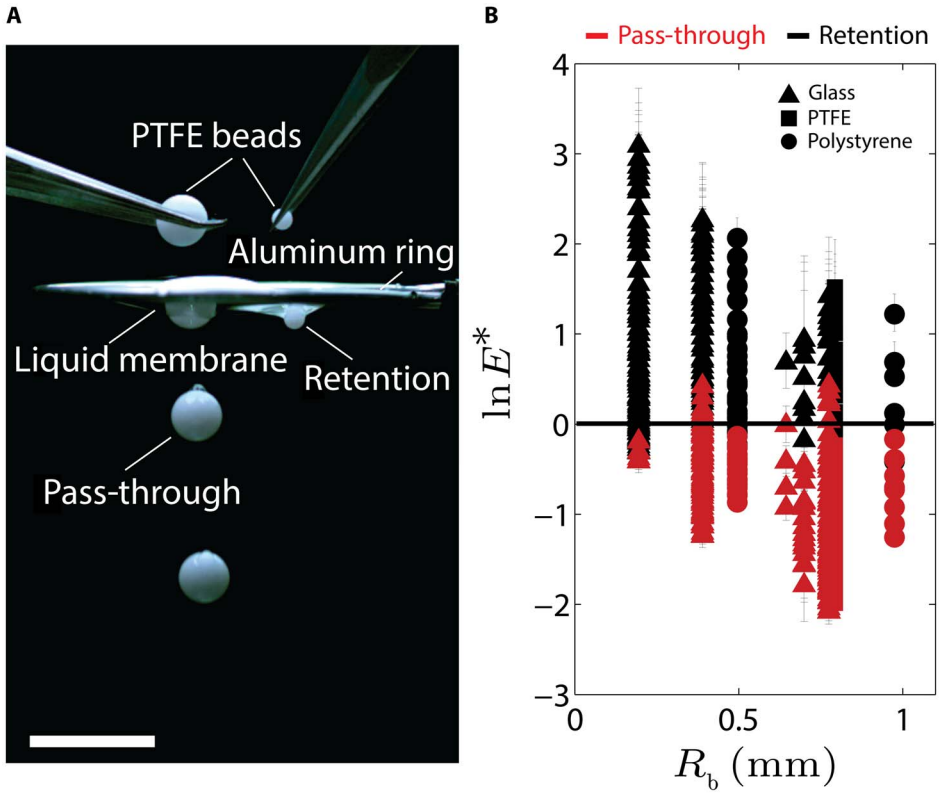

Fig. 2. Particle separation demonstration and membrane design. (**A**) This image is an overlay of four time-lapse images extracted from a video capturing two PTFE beads (one small and one large) falling into a liquid membrane at the same time from the same drop height. Tweezers used to hold the beads here were only shown for the image before the beads were released for clarity. (**B**) Data from 718 independent bead drop experiments used to determine the criteria for retention versus pass-through (each marker represents an individual bead drop event, and the error bars indicate the possible errors resulting from the measurements of physical parameters in Eq. 3). Scale bar, 1 cm.

where $C = \pi\{R_b^2[\sinh\phi + \phi] - 2(R_f^2 - R_b^2)\}$ is a geometry term. Conceptually, Eq. 3 is the ratio of energy converted to surface energy and the kinetic energy at impact. It is important to note that E^* accounts for shape deformation of a liquid membrane that is not captured by the conventional Weber number—a dimensionless number typically representing the relative importance of the kinetic energy of an impacting liquid droplet and its surface energy (*14*). On the basis of 718 independent bead dropping experiments, we generally observe that particles are retained when $E^* > \sim 1$ and pass through when $E^* < \sim 1$ for all particle surface chemistries used here (Fig. 2B), provided that the weight F_g of the bead does not exceed the capillary force the film can exert on the bead (F_γ) (that is, $F_g < F_\gamma$; we note that Eq. 3 may not be applicable when aggregation of smaller particles occurs, creating an effectively large particle, which could lead to $F_g > F_\gamma$). That is, there is an E^* value that separates the particle retention and particle pass-through regimes and that describes the conditions under which a particle will pass through or be blocked by the membrane. This further highlights the fact that the particle separation physics of a liquid membrane are different from those of a solid membrane. Therefore, E^* (that is, Eq. 3) can be used as a simple criterion to categorize the particle separation regimes of the liquid film for smooth beads with negligible dissipation effects.

Potential applications I: Insect and particle barrier

From a materials design perspective, the above criterion allows us to design a membrane (that is, γ and R_f) that can retain particles smaller than a critical size given the inertial properties of the impacting particles (that is, ρ_b and u_b; movie S2 and fig. S3). This capability can also be extended from simple particles to living organisms. For example, the typical speed of certain air particulates such as pollen or dust (with densities <2 g/cm^3) is <1 m/s; using these values, we predict that objects of size <1 mm can be retained in membranes (35 mN/m) designed in our experiments (R_f = 1.5 cm). In this example, micro-/nanoscopic particles and contaminates (for example, pollen), as well as certain slow-moving, disease-carrying insects (for example, mosquitoes and gnats) would not pass through the liquid membrane (Fig. 3A). We have further verified this prediction by dropping a number of relevant insects (that is, fruit fly, housefly, and mosquito) at their typical locomotion speeds at impact (Fig. 3B and movie S3). Note that dead insects were used in these experiments to ensure that the impact speed is near the cruising speed of their live counterparts (table S5). To further demonstrate the effectiveness of these liquid membranes in retaining live flying insects, we allowed live fruit flies (wild-type *Drosophila melanogaster* Canton Special) to interact with a liquid membrane. This demonstration showed that liquid membranes can effectively prevent the passage of flying fruit flies (Fig. 3C and movie S4).

Potential applications II: Self-cleaning, nonfouling membrane for continuous particle separation

In addition to the unique size selectivity of liquid membranes, their mobile liquid interface offers unique capabilities that cannot be readily

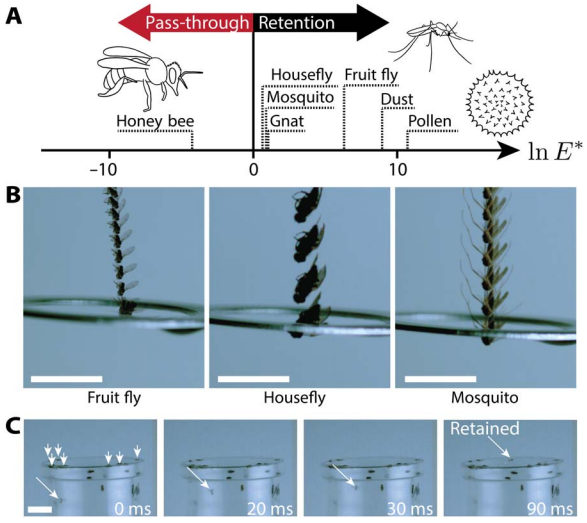

Fig. 3. Liquid membranes as selective microorganism and particulate barrier. (**A**) This plot shows the type of organisms that theoretically can pass through (or be retained by) a specified liquid membrane (with a radius of 1.5 cm and surface tension of ~35 mN/m) according to the value of E^* based on the characteristic size, locomotion speed, and mass or density of the organism of interests. (**B**) Demonstrations of retention of fruit flies (*Drosophila hydei*), houseflies (*Musca domestica*), and mosquitoes [*Culicidae (Diptera)*] by the liquid membranes at impact speeds of ~0.5, ~1.1, and ~0.9 m/s, respectively (see movie S3). Here, dead insects are used in an effort to control the impact velocity of the insect. Each panel represents an overlay of multiple images from one video to show insect position over time. (**C**) Time series of a live fruit fly flying into a liquid membrane (see movie S4). In the left panel, the short arrows point to fruit flies that have already been trapped in the membrane, and the long arrow points to the fruit fly of interest. In the next two panels, we see the fruit fly of interest flying up into the membrane, where it is retained in the last panel. Scale bars, 1 cm.

accomplished by any conventional synthetic membranes, including in-membrane object maneuverability (Fig. 4A and movie S5) and transport of retained particles by external forces (Fig. 4B and movie S6). These unique aspects of liquid membranes can be used to design separation membranes that resist fouling issues common for many solid-based membranes. Specifically, our liquid membranes can resolve the local membrane fouling issue in two separate ways. First, liquid membranes allow in-membrane object transport through external forces (for example, gravity), which allow contaminates to be transported away from the region of separation. Second, aggregates of the collected contaminates can be removed from the membrane once the weight of the aggregates exceeds the capillary force supported by the liquid membrane (Fig. 4C and movie S7). These unique mechanisms allow the liquid membranes to perform continuous separation without fouling.

Potential applications III: Surgical film

In addition, the simple yet unique capabilities of the free-standing liquid membranes could lend them the ability to provide out-of-the-box solutions to various problems, such as blocking contaminants for open surgery in regions where a dust-free space for safe surgical care is limited (*15*), or other applications involving blockage of small objects while allowing the passage of large devices. As a proof-of-concept demonstration of such an application, we showed that the liquid membrane can block contaminants during simulated surgical procedures without inhibiting visibility or maneuverability and can collect and remove contaminants (Fig. 4D and movie S8). In our demonstration, we were able to manipulate surgical tools within the membrane and pass bovine flesh from the simulated surgical opening through the membrane. Meanwhile, particles introduced to the membranes were trapped and diverted to the membrane edge due to the mobility of the liquid interface. In addition, we have shown quantitatively that these liquid membranes can successfully prevent contaminants from passing through them (Fig. 4E).

Potential applications IV: Gas/odor barrier

Another interesting aspect of the liquid membrane is that it can serve as a gas diffusion barrier (*16*, *17*) while allowing macroscopic objects to pass through it. Here, a gas diffusion barrier refers to a material that decreases the diffusivity of a gas compared to its diffusivity in air. This capability could be useful as a simple solution for solid waste/odor management in odor-concentrated environments. For example, making waterless toilets attractive from an olfactory perspective is an important factor toward addressing open defecation (*18*) practiced by ~1.1 billion people (as of 2015) (*19*). If liquid membranes can significantly decrease the rate of diffusion of chemicals relevant in waterless toilets, then they would be an inexpensive solution toward addressing the open defecation problem. To demonstrate the use of liquid membranes for the sequestration of gas while allowing the passage of solids, we first used fog produced by a humidifier to simulate and visualize gas, and used a suspended liquid film to block the fog while allowing solid objects to pass through the membrane (Fig. 5A and movie S9). Humidity measurements taken above an intact liquid membrane show that a liquid membrane can be as effective as an impermeable glass substrate (control) in blocking the fog passage (Fig. 5, B and C). To further demonstrate that the liquid membrane can serve as a gas diffusion barrier, we performed a similar experiment with a combustible gas. In this test, a test tube filled with hexane was placed near a gas sensor, and the hexane vapor was blocked with either a parafilm cover (control) or a liquid membrane (consisting of deionized water, glycerol, and SDS). Our test results have shown that the liquid membrane can be as effective as the parafilm cover to block the gas (Fig. 5, D and E). We note that the ability for a gas to pass through a liquid membrane depends on its ability to dissolve into the liquid itself and its chemical affinity for the surfactant used in the liquid membrane (*17*). A surfactant may be chosen such that it does not have a chemical affinity with the gas to be sequestered. Depending on the environment of interest, the composition of the liquid membranes will need to be engineered to accommodate a specific application.

DISCUSSION

Most applications for free-standing liquid membranes could only be realized if the membranes remain intact in the presence of perturbations expected in the application of interest over desired time frames. For example, typical surgical time for knee replacements is on the order of 2 to 3 hours (*20*), whereas typical defecation durations for humans are on the orders of seconds (diarrhea) to an hour (constipation) (*21*). In cases where evaporation or fluid loss due to wetting on impacting solids limits membrane longevity, membrane lifetime can be enhanced by using reservoirs for fluid replenishment. We have shown that, with a liquid reservoir, the hydrated liquid film can sustain >3000 cycles of film perturbations (over 3 hours) without rupture (Fig. 6, A and B, and movie S10). One may also tailor the composition of the liquid film by incorporating a number of hygroscopic molecules and other additives (*22*) to maximize longevity without liquid replenishment. As a proof-of-concept demonstration, we used a genetic algorithm (*23*–*25*) to develop liquid membrane compositions. Specifically, we used differential evolution (*23*) on mixtures composed of deionized water, glycerol,

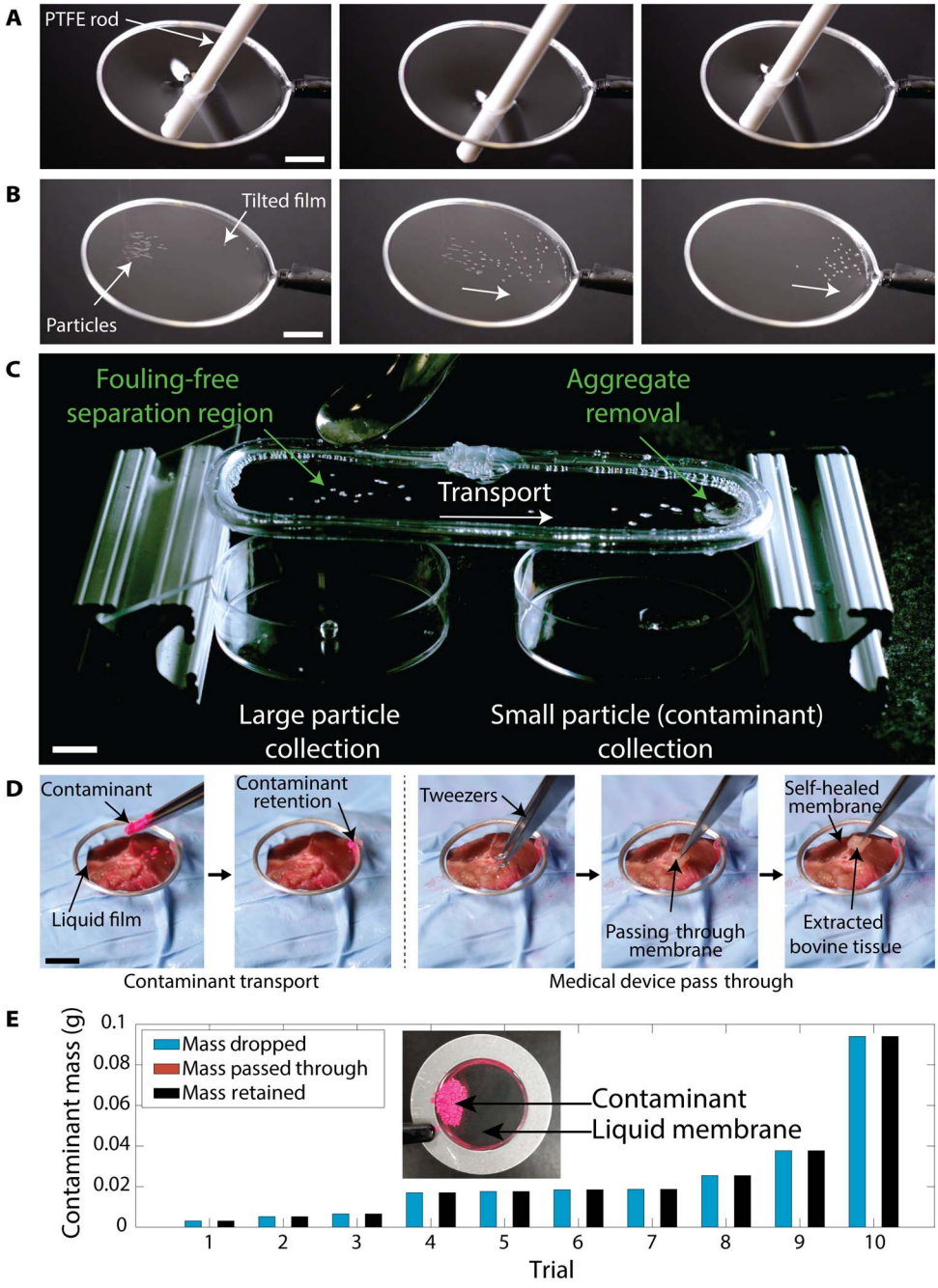

Fig. 4. Potential use of liquid membranes in nonfouling particle separation and surgery. (**A**) Dynamic reconfigurability: Unlike those in solid membranes, objects embedded in the liquid membranes can move freely in the plane of the membrane due to the mobility of the liquid molecules (see movie S5). (**B**) Particle transport: Particles retained in the film can also move within the plane of the liquid membrane, allowing them to be transported away if needed (see movie S6). Note also that these particular liquid membranes are transparent, allowing them to be used in applications requiring through-film visibility. (**C**) Self-cleaning of liquid membranes: Here, a tilted liquid membrane passively removes contaminates (that is, small sand particles) from the separation region by gravity, allowing the large particle to be collected in the left petri dish. The small particles are collected downstream, forming a growing aggregate that will later fall from the membrane into the petri dish on the right when the weight of the aggregates exceeds the capillary force exerted by the liquid membrane ("aggregate removal"; see movie S7). (**D**) Simulated surgery: We demonstrated that the liquid membrane can block contaminants during simulated surgical procedures without inhibiting visibility or in-film maneuverability and can passively and continuously collect and remove contaminants (see movie S8). (**E**) Plot showing the retention of various amounts of contaminants on a liquid membrane. Note that, in all the trials, no measurable amount of contaminant leaked through the membranes and, therefore, no data are shown for the red data bar representing "mass passed through." The contaminant was different quantities of fluorescent powder [the same as that used in (D)] sprinkled from a drop height of ~1 cm. Scale bars, 1 cm.

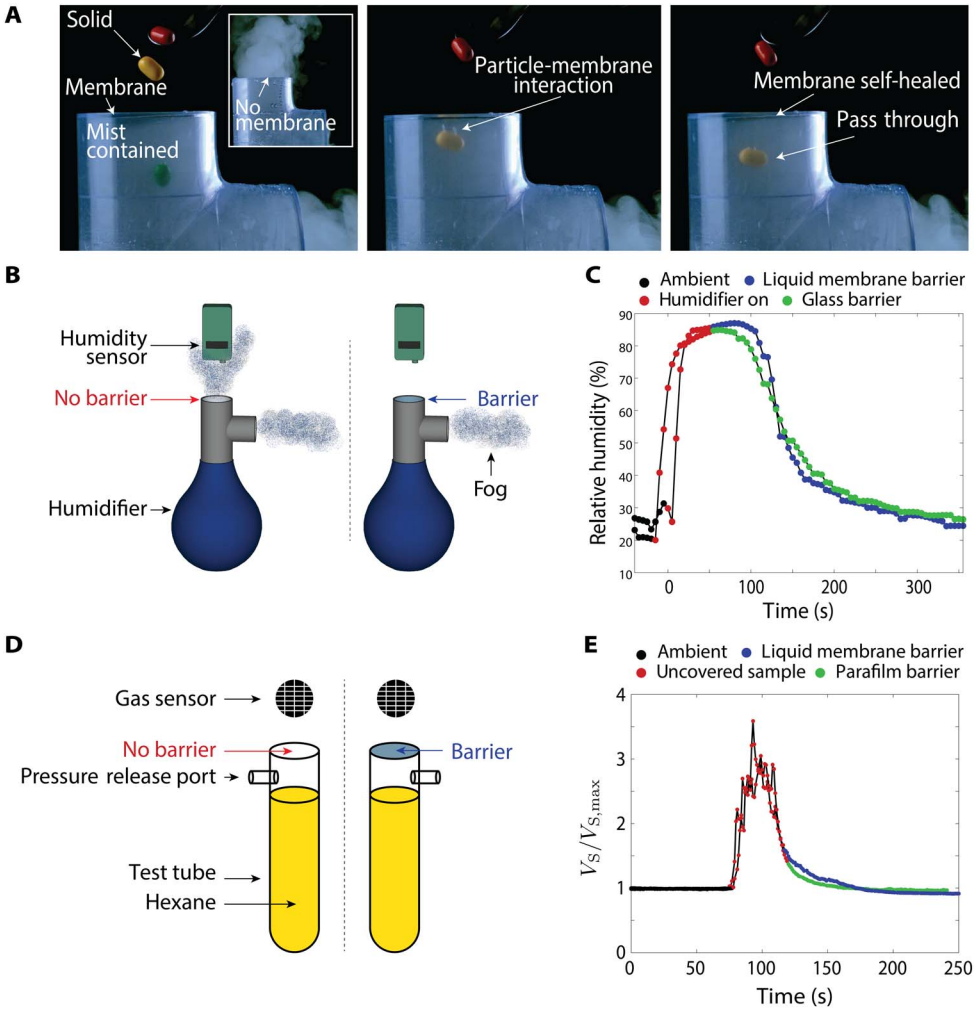

Fig. 5. Potential use of liquid membranes as selective solid/gas filters. (**A**) A liquid film can serve as a gas diffusion barrier while allowing macroscopic objects to pass through (for example, odor management; see movie S9). (**B**) Schematic of the experimental setup in assessing the ability of a liquid membrane (barrier) to prevent the passage of fog. (**C**) Quantitative measurements showing that a liquid membrane can be as effective as a solid glass barrier in blocking the fog passage. (**D**) Gas sequestration experimental setup. Here, a hexane-filled test tube was covered with either parafilm or a liquid membrane. (**E**) The measured sensor output (signal voltage V_s normalized by the maximum voltage in ambient conditions, $V_{s,max}$) over time when exposed to ambient (black circles) and hexane vapor (red circles) and when covered by either a parafilm sheet (green circles) or a liquid membrane (blue circles). The liquid membrane consists of a 7:3 ratio of deionized water to glycerol by volume and 8.5 mM SDS.

SDS, tannic acid (*22*), and polyethylene oxide (PEO) and used the average longevity (that is, time between film formation and film rupture) for the selection phase of the genetic algorithm. Some of these components (glycerol, tannic acid, and PEO) are well-known hygroscopic agents. On the basis of these chemical components, we were able to generate a liquid membrane composition that lasted for an average of 64 min (25 measurements) with a maximum observed longevity of 6.5 hours under room conditions (temperature of 22.3°C, 49% relative humidity) without liquid replenishment. Therefore, it is possible to optimize the film compositions (*24*) to create long-lasting membranes using advanced experimental design methods to meet various application requirements.

To further understand how liquid membranes may behave under mechanical perturbations, we investigated the robustness of these liquid membranes under periodic vibrations. In our tests, arrays of liquid membranes (R_f ~1 cm) were perturbed simultaneously at different frequencies through a mechanical vibration system (fig. S4). Our results showed that membrane lifetime highly depends on the frequency of external perturbations. For example, certain frequencies (for example, 55 Hz) promote ejection of liquid droplets from the membrane and are thus destructive, whereas other frequencies (for example, ~80 to 85 Hz) appear to have little effect on the membrane lifetime. Systematic study of the influence of mechanical perturbations on the liquid membrane longevity with respect to different liquid membrane compositions and dimensions will enable us to tailor liquid membrane compositions suitable for specific applications.

Note that our current study mainly focuses on the interaction of relatively smooth (that is, $\xi < \sim 2.5\ \mu m$), spherical beads with liquid membranes in an effort to understand particle selectivity. Through our high-speed camera imaging on the bead-film interaction, we observed that the contact line dynamics of the liquid membrane play an important role in the film rupture and retention of residual liquid around the particle. For example, satellite droplets can always be observed on top of both hydrophobic and hydrophilic smooth beads as the liquid film detaches from the bead surface (fig. S5). Further investigations on the effect of surface roughness and particle shape on the membrane-solid interactions and

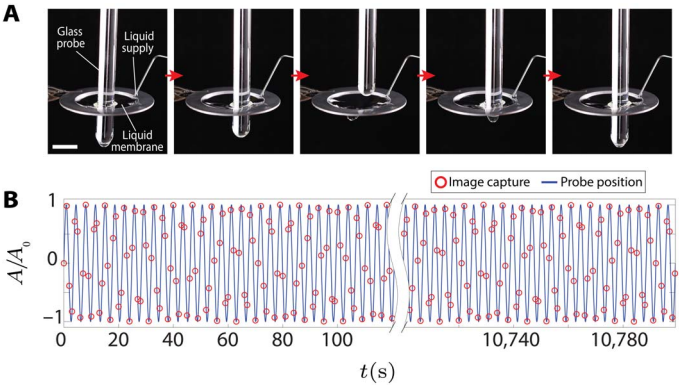

Fig. 6. Longevity and mechanical perturbation of a liquid membrane. (**A**) Time sequence of images showing the mechanical perturbation of a liquid membrane by a smooth glass rod for >3 hours. Probing took place at a period of 3.55 s over 3042 cycles (see movie S10), and liquid was replenished at a rate of ~1 to 2 ml/min. We note that the glass rod is hydrophilic, so some liquid from the membrane wets its surface as it passes into the membrane repeatedly. Scale bar, 1 cm. (**B**) Plot showing the mechanical perturbation cycle of the liquid membrane. The experiment was set up to acquire images at various points in the cycles (shown in red open circles). Images were acquired at a rate of 1 frame/s. Note that A is the vertical location of the probe tip, and A_0 is the amplitude of the probing cycle.

the mechanics of membrane rupture may enable us to design physically sturdy membranes for highly demanding applications.

With the availability of a wide spectrum of soluble functional molecules, advanced liquid membranes could be designed by incorporating these molecules to tailor membrane gas permeability, rheological properties, conductivity, insect repellency, antiseptic properties, or any other desired functions for targeted applications. It is anticipated that the unique nature of free-standing liquid membranes may open up novel and creative technological applications in medicine, waste management, pest and disease control, and other applications beyond the reach of current membrane technologies.

MATERIALS AND METHODS

Surface tension and density of liquid membrane solution

The surface tension γ of the liquid membranes as a function of concentration of SDS is shown in table S1. These measurements were obtained using the pendant drop method with a ramé-hart goniometer and DROPimage software or DropSnake software (*26*). The density ρ_f of each liquid membrane solution was determined by measuring the mass of a given volume of the solution. The results are also shown in table S1.

Mass and thickness of liquid membrane

In an effort to understand variation between individual liquid membranes, we measured the mass m of 5 to 10 freshly formed liquid membranes. As a rough estimate of liquid membrane thickness, the membrane of volume V and density ρ_f was assumed to be a thin cylinder with a radius R_f (the ring radius). With this in mind, the film thickness τ was calculated as follows

$$\tau = \frac{m}{\rho_f \pi R_f^2}$$

Estimated initial film thicknesses based on this equation are shown in table S2. This estimation represents an approximation of the initial film thickness here because some liquid volume may be collected near the film perimeter due to wetting of the liquid on the hydrophilic aluminum ring.

Bead roughness

Roughness measurements of the beads used in our experiments and of flat surfaces used for contact angle measurements were performed using an optical profilometer (ZYGO Nexview). Here, roughness ξ is defined as the root mean square roughness. Using this instrument, we conducted roughness measurements on six different regions of both flat and spherical samples of PTFE, PS, and glass. The average and SD of these six values of ξ are shown in table S3.

Wetting characteristics of liquid membrane solution on bead material

Contact angle measurements of liquid membrane films on flat surfaces composed of materials chemistry similar or identical to that of the beads used in our experiments were used to approximate the energy loss due to pinning (section S2 and figs. S1 and S2). To approximate the energy dissipation associated with pinning, both advancing and receding contact angle values were required. Because the surface roughnesses of our flat surface samples are smaller than those of the beads (table S3), this would lead to an underestimate of the energy dissipation due to liquid pinning. To calculate an upper estimate of the pinning energy for an order of magnitude comparison, we assumed the receding angles to be zero in all cases (that is, $\theta_R = 0°$). The experimentally measured advancing angles are shown in table S4.

Inertial characteristics of living organisms and particles

In Fig. 3A, we calculated the value of E^* based on the mass or density, characteristic size, and typical speed reported for each organism/particle (table S5). We assumed that the film had a radius of $R_f = 1.5$ cm, and the surface tension was 35.6 mN/m (that is, the smallest surface tension we tested). We conducted housefly size and mass measurements, which are included in table S5. Insects used for measurements and for the insect dropping tests shown in Fig. 3B were all purchased from DeadInsects.Net.

Humidity sensing

The relative humidity of the space ~3 cm above the humidifier (Crane Ultrasonic Cool Mist) outlet was measured over time (every 5 s) to compare the local relative humidity in the presence and absence of a liquid membrane or a glass dish (control). Because the humidifier causes a flow of air, a side-facing exit of the piping was needed to prevent the liquid membrane from developing curvature.

Gas sensing

The concentration of hexane vapor was measured in the space above a test tube filled with hexane (vapor pressure of ~17.6 kPa at 20°C; Sigma-Aldrich) using an MQ-135 gas sensor module (All Electronics). The test tube was covered with either parafilm (control) or a liquid membrane. The hexane vapor pressure increased gradually over time when covered, causing the radius of curvature of the liquid membrane to decrease over time, necessitating a pressure release port (a long tube with an outlet extending ~30 cm away from sensor) in this specific experiment.

Mechanical vibration test

In this experiment, a PASCO mechanical wave driver oscillating vertically at an amplitude of ~3 mm was connected to a metal plate with an

array of circular cutouts 2 cm in diameter. This setup was used to perturb liquid membranes at set frequencies. Liquid membranes consisting of water, glycerol, and SDS were applied to the holes. A video camera was used to assess the membrane longevity.

Genetic algorithm

A free-standing liquid membrane can be composed of various different components, and different formulations may have different properties. For example, one composition may typically have a longer lifetime than others. In an effort to create a long-lasting liquid membrane and to demonstrate how liquid membranes might be tailored to meet the needs of various applications, we used a genetic algorithm called differential evolution (*23*), an algorithm that has been successfully implemented in other experimental studies (*25*). For our experiments, we used deionized water, glycerol, tannic acid (*22*), PEO, and SDS as components of the liquid membranes and selected for average liquid membrane longevity. These additives were chosen because of their hygroscopic or stabilizing properties. Our component concentration search ranges (min/step size/max) were as follows: deionized water (0 ml/5 ml/40 ml), SDS (0 mM/1.7 mM/15.6 mM), tannic acid (0 mM/0.3 mM/2.9 mM), PEO (0 g/.09 g/1.0 g in 40 ml of solution), and glycerol (40 ml minus the volume of deionized water for the given formulation).

The search for the composition with the longest average longevity had five compositions per generation ($NP = 5$), with four components ($D = 4$; glycerol not considered, as its volume is dependent on the water volume). The first generation of compositions was determined by random number generation for each component. To determine the next generation, we used the equations outlined by Storn and Price (*23*), using a crossover constant of 0.5 ($CR = 0.5$) and a step size of 0.5 ($F = 0.5$) to generate a set of test compositions. We then compared the average longevity of each composition $X_{i,G}$ ($i = 1, 2, \ldots D$; G denotes the generation) to that of the respective test composition $U_{i,G}$. Composition $X_{i,G+1}$ was determined to be either composition $X_{i,G}$ or composition $U_{i,G}$: The composition with the higher average longevity was chosen to be $X_{i,G+1}$. Note that it is possible to select for other properties to achieve a liquid membrane of interest. For example, instead of selecting for average longevity, it is possible to select for maximum longevity, number of perturbations before rupture, bactericidal effectiveness, or other properties desired for the liquid membrane. We measured the longevity of 72 different compositions. For each of those compositions, we formed up to 59 membranes in parallel for statistical purposes and measured their longevity. The total volume of the solutions was kept constant (40 ml).

SUPPLEMENTARY MATERIALS

Supplementary material for this article is available at http://advances.sciencemag.org/cgi/content/full/4/8/eaat3276/DC1

Section S1. Descriptions of movies S1 to S10
Section S2. Sources of energy dissipation
Fig. S1. A schematic diagram showing a bead passing through a liquid membrane.
Fig. S2. Comparison of the relative magnitude of different energy terms.
Fig. S3. Theoretical dependence of E^* on relevant parameters.
Fig. S4. Effect of mechanical perturbation frequency on the longevity of liquid membranes.
Fig. S5. Residual liquid on both hydrophilic and hydrophobic particles.
Table S1. Surface tension and density of different liquid membrane solutions.
Table S2. Liquid membrane mass and thickness characterization.
Table S3. Surface roughness measurements of various bead materials.
Table S4. Advancing angles of liquid membrane solution droplets on a flat surface.
Table S5. Reported inertial parameters for various organisms and particles.
Movie S1. Large and small bead separation.
Movie S2. Particle filtration.
Movie S3. Insect retention.
Movie S4. Live insect retention.
Movie S5. In-film probe movement.
Movie S6. Particle transport.
Movie S7. Self-cleaning of liquid membranes.
Movie S8. Simulated surgery.
Movie S9. Liquid membranes as selective gas/solid barriers.
Movie S10. Liquid membrane longevity.
References (*27*–*40*)

REFERENCES AND NOTES

1. P. Yager, T. Edwards, E. Fu, K. Helton, K. Nelson, M. R. Tam, B. H. Weigl, Microfluidic diagnostic technologies for global public health. *Nature* **442**, 412–418 (2006).
2. J. R. Werber, C. O. Osuji, M. Elimelech, Materials for next-generation desalination and water purification membranes. *Nat. Rev. Mater.* **1**, 16018 (2016).
3. S. J. Singer, G. L. Nicolson, The fluid mosaic model of the structure of cell membranes. *Science* **175**, 720–731 (1972).
4. S. K. Y. Tang, W. F. Marshall, Self-repairing cells: How single cells heal membrane ruptures and restore lost structures. *Science* **356**, 1022–1025 (2017).
5. T.-S. Wong, S. H. Kang, S. K. Y. Tang, E. J. Smythe, B. D. Hatton, A. Grinthal, J. Aizenberg, Bioinspired self-repairing slippery surfaces with pressure-stable omniphobicity. *Nature* **477**, 443–447 (2011).
6. A. K. Epstein, T.-S. Wong, R. A. Belisle, E. M. Boggs, J. Aizenberg, Liquid-infused structured surfaces with exceptional anti-biofouling performance. *Proc. Natl. Acad. Sci. U.S.A.* **109**, 13182–13187 (2012).
7. P. Kim, T.-S. Wong, J. Alvarenga, M. J. Kreder, W. E. Adorno-Martinez, J. Aizenberg, Liquid-infused nanostructured surfaces with extreme anti-ice and anti-frost performance. *ACS Nano* **6**, 6569–6577 (2012).
8. X. Yao, Y. Hu, A. Grinthal, T.-S. Wong, L. Mahadevan, J. Aizenberg, Adaptive fluid-infused porous films with tunable transparency and wettability. *Nat. Mater.* **12**, 529–534 (2013).
9. X. Hou, Y. Hu, A. Grinthal, M. Khan, J. Aizenberg, Liquid-based gating mechanism with tunable multiphase selectivity and antifouling behaviour. *Nature* **519**, 70–73 (2015).
10. C. Isenberg, *The Science of Soap Films and Soap Bubbles* (Dover Publications Inc., 1978).
11. L. Courbin, H. A. Stone, Impact, puncturing, and the self-healing of soap films. *Phys. Fluids* **18**, 091105 (2006).
12. A. Le Goff, L. Courbin, H. A. Stone, D. Quéré, Energy absorption in a bamboo foam. *Europhys. Lett.* **84**, 36001 (2008).
13. T. Killian, J. Huey, J. Bryson, T. Truscott, Self healing soap films. https://arxiv.org/abs/1210.3797 (2013).
14. Y. A. Çengel, J. M. Cimbala, *Fluid Mechanics* (McGraw-Hill, ed. 3, 2014).
15. S. S. Chawla, S. Gupta, F. M. Onchiri, E. B. Habermann, A. L. Kushner, B. T. Stewart, Water availability at hospitals in low- and middle-income countries: Implications for improving access to safe surgical care. *J. Surg. Res.* **205**, 169–178 (2016).
16. H. M. Princen, S. G. Mason, The permeability of soap films to gases. *J. Colloid Sci.* **20**, 353–375 (1965).
17. S. Cohen-Addad, D. Quéré, Permeability of a soap film, in *Soft Order in Physical Systems*, Y. Rabin, R. Bruinsma, Eds. (Plenum Press, 1994), pp. 195–198.
18. J. Lin, J. Aoll, Y. Niclass, M. I. Velazco, L. Wünsche, J. Pika, C. Starkenmann, Qualitative and quantitative analysis of volatile constituents from latrines. *Environ. Sci. Technol.* **47**, 7876–7882 (2013).
19. World Health Organization, *World Health Statistics 2015* (World Health Organization, 2015).
20. J. Zhou, F. Dexter, A. Macario, D. A. Lubarsky, Relying solely on historical surgical times to estimate accurately future surgical times is unlikely to reduce the average length of time cases finish late. *J. Clin. Anesth.* **11**, 601–605 (1999).
21. P. J. Yang, M. LaMarca, C. Kaminski, D. I. Chu, D. L. Hu, Hydrodynamics of defecation. *Soft Matter* **13**, 4960–4970 (2017).
22. G. A. Cook, Tough soap films and bubbles. *J. Chem. Educ.* **15**, 161 (1938).
23. R. Storn, K. Price, Differential evolution—A simple and efficient heuristic for global optimization over continuous spaces. *J. Glob. Optim.* **11**, 341–359 (1997).
24. P. K. Wong, F. Yu, A. Shahangian, G. Cheng, R. Sun, C.-M. Ho, Closed-loop control of cellular functions using combinatory drugs guided by a stochastic search algorithm. *Proc. Natl. Acad. Sci. U.S.A.* **105**, 5105–5110 (2008).
25. H. Tsutsui, B. Valamehr, A. Hindoyan, R. Qiao, X. Ding, S. Guo, O. N. Witte, X. Liu, C.-M. Ho, H. Wu, An optimized small molecule inhibitor cocktail supports long-term maintenance of human embryonic stem cells. *Nat. Commun.* **2**, 167 (2011).

26. A. F. Stalder, G. Kulik, D. Sage, L. Barbieri, P. Hoffmann, A snake-based approach to accurate determination of both contact points and contact angles. *Coll. Surf. A Physicochem. Eng. Asp.* **286**, 92–103 (2006).
27. C. G. L. Furmidge, Studies at phase interfaces. I. The sliding of liquid drops on solid surfaces and a theory for spray retention. *J. Colloid Sci.* **17**, 309–324 (1962).
28. L. M. Sosnoskie, T. M. Webster, D. Dales, G. C. Rains, T. L. Grey, A. S. Culpepper, Pollen grain size, density, and settling velocity for Palmer amaranth (*Amaranthus palmeri*). *Weed Sci.* **57**, 404–409 (2009).
29. J. S. Borrell, Rapid assessment protocol for pollen settling velocity: Implications for habitat fragmentation. *Biosci. Horizons* **5**, hzs002 (2012).
30. World Health Organization, *Hazard Prevention and Control in the Work Environment: Airborne Dust* (World Health Organization, 1999).
31. C. R. Martin, Characterization of grain dust properties. *Trans. ASAE* **24**, 738–742 (1981).
32. Y. Sun, S. N. Fry, D. P. Potasek, D. J. Bell, B. J. Nelson, Characterizing fruit fly flight behavior using a microforce sensor with a new comb-drive configuration. *J. Microelectromech. Syst.* **14**, 4–11 (2005).
33. S. B. Fuller, A. D. Straw, M. Y. Peek, R. M. Murray, M. H. Dickinson, Flying *Drosophila* stabilize their vision-based velocity controller by sensing wind with their antennae. *Proc. Natl. Acad. Sci. U.S.A.* **111**, E1182–E1191 (2014).
34. W. B. Worthen, Latitudinal variation in developmental time and mass in *Drosophila melanogaster*. *Evolution* **50**, 2523–2529 (1996).
35. A. K. Dickerson, P. G. Shankles, N. M. Madhavan, D. L. Hu, Mosquitoes survive raindrop collisions by virtue of their low mass. *Proc. Natl. Acad. Sci. U.S.A.* **109**, 9822–9827 (2012).
36. A. Ahmad, V. R. Rao, P. R. Krishna, On speed and aerodynamic forces of mosquito. *Indian J. Exp. Biol.* **38**, 766–771 (2000).
37. D. H. Akey, H. W. Potter, R. H. Jones, Effects of rearing temperature and larval density on longevity, size, and fecundity in the biting gnat *Culicoides variipennis*. *Ann. Entomol. Soc. Am.* **71**, 411–418 (1978).
38. H. Tennekes, *The Simple Science of Flight: From Insects to Jumbo Jets* (MIT Press, 2009).
39. C. Wehrhahn, T. Poggio, H. Bülthoff, Tracking and chasing houseflies (*Musca*). *Biol. Cybern.* **45**, 123–130 (1982).
40. M. L. Winston, *The Biology of the Honey Bee* (Harvard Univ. Press, 1991).

Acknowledgments: We thank A. P. Blois and K. Hannon for the initial involvement of the project. We also thank B. Cheng, R. Ordway, and P. Liu for the help with the live fruit fly experiments. **Funding:** We acknowledge funding support by NSF CAREER Award No. 1351462 and the Wormley Family Early Career Professorship. B.B.S. acknowledges support from the NSF Graduate Research Fellowship (grant no. DGE1255832). Part of the work was conducted at the Penn State node of the NSF-funded National Nanotechnology of Infrastructure Network. **Author contributions:** B.B.S. and T.-S.W. conceived and designed the experiments. B.B.S. and L.G. performed bead dropping experiments. B.B.S. and H.F. performed wetting and surface tension characterizations. J.W. performed surface roughness measurements. B.B.S., L.G., H.F., and H.C. performed film longevity tests. B.B.S. conducted data analysis and theoretical modeling. B.B.S. and T.-S.W. wrote the manuscript. **Competing interests:** B.B.S. and T.-S.W. are inventors on a patent application related to this work filed by the Penn State Research Foundation (application no. 62/490,068; filed on 26 April 2017). The authors declare no other competing interests. **Data and materials availability:** All data needed to evaluate the conclusions in the paper are present in the paper and/or the Supplementary Materials. Additional data related to this paper may be requested from the authors.

Submitted 14 February 2018
Accepted 17 July 2018
Published 24 August 2018
10.1126/sciadv.aat3276

Citation: B. B. Stogin, L. Gockowski, H. Feldstein, H. Claure, J. Wang, T.-S. Wong, Free-standing liquid membranes as unusual particle separators. *Sci. Adv.* **4**, eaat3276 (2018).